NANOROBOTS

A DNA molecular printer capable of programmable positioning and patterning in two dimensions

Erik Benson[1,2], Rafael Carrascosa Marzo[1,2], Jonathan Bath[1,2], Andrew J. Turberfield[1,2]*

Nanoscale manipulation and patterning usually require costly and sensitive top-down techniques such as those used in scanning probe microscopies or in semiconductor lithography. DNA nanotechnology enables exploration of bottom-up fabrication and has previously been used to design self-assembling components capable of linear and rotary motion. In this work, we combine three independently controllable DNA origami linear actuators to create a nanoscale robotic printer. The two-axis positioning mechanism comprises a moveable gantry, running on parallel rails, threading a mobile sleeve. We show that the device is capable of reversibly positioning a write head over a canvas through the addition of signaling oligonucleotides. We demonstrate "write" functionality by using the head to catalyze a local DNA strand–exchange reaction, selectively modifying pixels on a canvas. This work demonstrates the power of DNA nanotechnology for creating nanoscale robotic components and could find application in surface manufacturing, biophysical studies, and templated chemistry.

INTRODUCTION

The vision of future technologies for atomically precise manufacturing is built on the assumption that materials and devices can be built, from the bottom up, by chemical reactions orchestrated by precise physical manipulation of atomic or molecular components (*1*, *2*). Picometer-scale control of motion can be achieved by macroscopic devices such as the piezoelectric actuators used in scanning probe manipulation (*3*, *4*). However, top-down nanopositioning technology is costly with very limited scalability (*5*). A principal focus of molecular nanotechnology is the construction of synthetic machinery that can manipulate matter at the nanoscale with the parallelism intrinsic to molecular systems. DNA nanotechnology is one of the most robust techniques for bottom-up assembly of complex nanostructures (*6*). Specifically, DNA origami, where a long DNA strand of (usually) biological origin is folded by hybridization to hundreds of short, synthetic oligonucleotides, can be used to create complex nanoscale objects with high resolution and yield (*7*). The origami technique has been used to produce a number of mechanical modules: mechanically interlocked slider rails (*8*–*11*), rotary arms (*12*, *13*), hinges (*14*), and closable containers (*15*). DNA nanostructures have been engineered to respond to external stimuli including signaling oligonucleotides by means of strand-exchange reactions (*15*, *16*); light (*17*), electric (*12*), and magnetic fields (*18*); changes in chemical environment (*19*, *20*); and the specific binding of target molecules (*21*, *22*).

Here, we combine three DNA origami linear actuators to construct a machine capable of two-dimensional (2D) positioning. Our designs draw inspiration from the vision of atomically precise manufacture through molecular manipulation (*1*) and from macroscopic printers. We demonstrate that the machine can be locked at programmed locations by the introduction of signaling oligonucleotides ("signal strands") and that this can be reversed by the introduction of release strands. We functionalize the moving carriage with a hybridization catalyst to create a write head and demonstrate programmed patterning of a molecular canvas using an all-DNA system.

RESULTS

Design and assembly of DNA positioning devices

A DNA origami nanostructure comprises a multi-kilobase scaffold hybridized to hundreds of staple strands, synthetic oligonucleotides that each bind two or more distinct domains of the scaffold to fold it into the desired structure of parallel helices held together by staple crossovers (*7*, *23*). The origami architecture enables fabrication of a wide range of structural forms by self-assembly, programmed through staple design. We have explored two architectures for our molecular printer, based on Cartesian and polar coordinate systems, shown in Fig. 1. The Cartesian printer is described in detail below; characterization of the polar device is presented in the Supplementary Materials.

A core constraint for DNA origami designs is the available scaffold material: Typical scaffolds derived from the single-stranded genome of bacteriophage M13 limit most origami structures to around 8000 base pairs (bp). Larger structures can be assembled from multiple DNA origami components (*24*). We chose to assemble our machines from three components: a flat canvas, a bounding frame with sliding crossrail (gantry), and a small origami sleeve (carriage) that moves along the rail (Fig. 1). The canvas is a rectangular 2D origami comprising 30 helices that run parallel to its long dimension. The frame comprises three nine-helix bundle beams linked by flexible scaffold regions. Two of the beams are connected to the short ends of the canvas (the helix ends) by hybridization of complementary 8–nucleotide (nt) extensions of frame and canvas staples (fig. S1); this forms the base of the printer. The circular scaffold of the frame runs from one base beam to the other along one long edge of the canvas, forming a 31st helix where it links to the canvas through ten 3-nt staple crossovers. The scaffold returns through a third nine-helix bundle, the rail, via single-stranded scaffold domains, which form flexible linkers between rail and base beams. The sleeve is formed from a 22-helix origami sheet with three double-layer regions. Three 18-nt strands, protruding from its inside, are designed to load the sleeve onto three complementary

[1]Department of Physics, University of Oxford, Clarendon Laboratory, Oxford, UK. [2]The Kavli Institute for Nanoscience Discovery, University of Oxford, New Biochemistry Building, Oxford, UK.
*Corresponding author. Email: andrew.turberfield@physics.ox.ac.uk

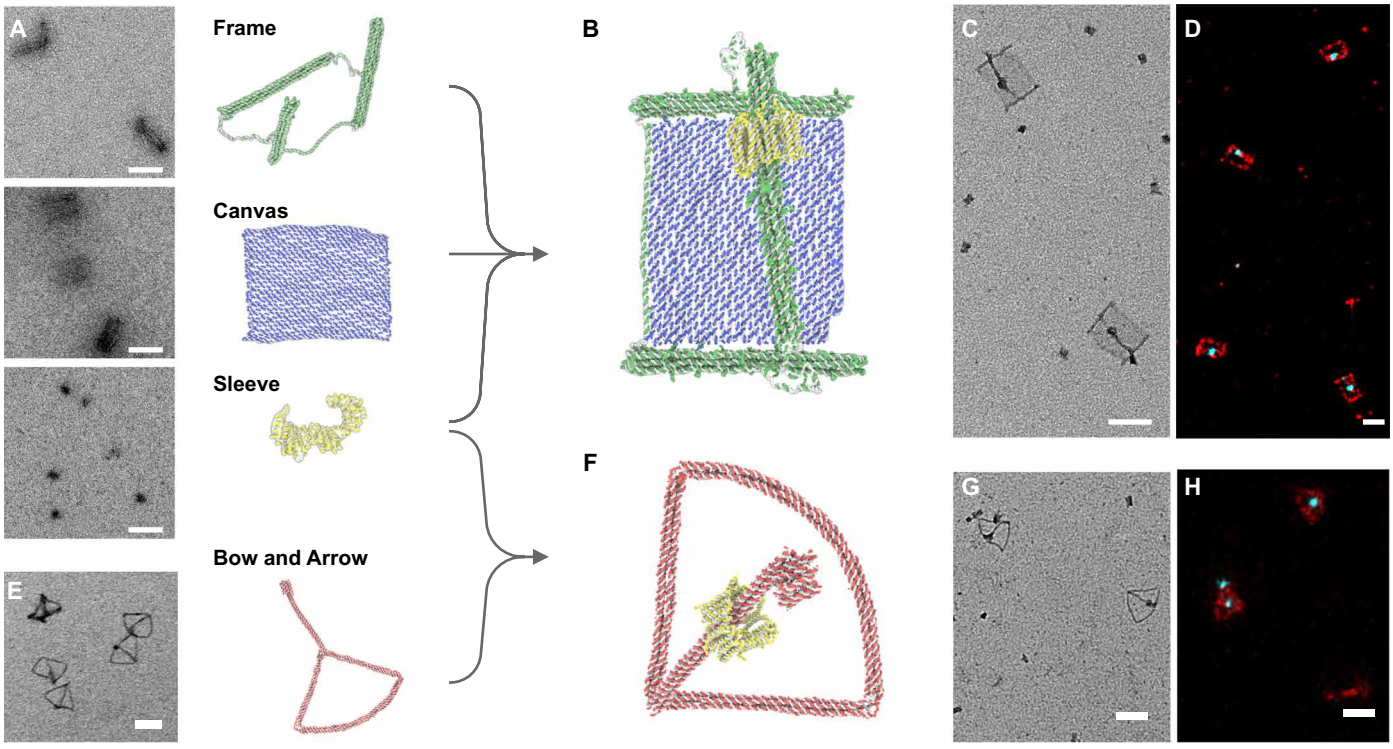

Fig. 1. DNA apparatus for 2D positioning. (**A**) Three independent DNA origami components: frame, canvas, and sleeve. Left, TEM; right, rendering of snapshots from oxDNA simulations. (**B**) When mixed, the three components assemble to form a Cartesian two-axis positioner: The crossrail moves along parallel side beams and spans the central canvas; the sleeve moves along the rail. Rendered images are snapshots of oxDNA (*29*, *30*) simulations. Assembled positioners are characterized by (**C**) TEM (free sleeves are also visible) and (**D**) DNA-PAINT (frame and canvas, red; sleeve, blue). (**E** to **H**) A polar positioning device assembled from "bow and arrow" frame and the same sleeve. All scale bars, 100 nm.

protruding strands in the middle of the central rail (fig. S2). The sleeve can be closed through the introduction of seam staple strands that link its two long edges, locking it around the rail. The canvas and frame are full-size origamis; the sleeve is constructed using a 1496-nt scaffold restriction digest fragment.

The three components were separately folded and purified by polyethylene glycol (PEG) precipitation (*25*) and characterized with transmission electron microscopy (TEM; Fig. 1A) and gel electrophoresis (fig. S3). The machine was assembled by mixing and incubating all components for 72 hours at 37°C followed by addition of seam strands to close the sleeve around the rail. Invader strands were then added to release the loading strands, locking the sleeve to the rail, freeing it to move along the rail. Polythymine-functionalized magnetic beads were used to bind polyadenine extensions to two staples of the sleeve. After closing and releasing the sleeve, the assembled devices were incubated with the beads, which were then washed to remove assemblies (frames and canvases) lacking sleeves. Bound structures were released from the beads by incubation with a polythymine invader strand. This procedure selected complete devices incorporating frame, canvas, and sleeve as well as free sleeves (Fig. 1C). Devices were immobilized on streptavidin-coated glass coverslips within flow cells via biotin covalently attached to staples at the base of the frame beams; during subsequent processing free sleeves were washed away. Immobilized devices were imaged by subdiffraction limit optical microscopy using DNA-PAINT (*26*) to localize fluorescent oligonucleotides transiently bound to single-stranded anchorages on the origami structure. PAINT docking sites are positioned on the three beams of the frame and in two lines along the canvas (Fig. 1D). PAINT docking sites with a different base sequence allow subsequent measurement of the sleeve position by replacing the imager strand solution (*27*).

In initial experiments, the eight protrusions linking the frame to the short edges of the canvas formed weaker links, 6 bp rather than 8 bp. Gel electrophoresis and TEM of frame-canvas mixtures confirmed correct insertion of the canvas in the frame, but at subnanomolar concentrations (after gel purification), the yield of complete structures was low. When devices were bound to a glass surface and imaged with DNA-PAINT, most frames no longer had a canvas attached. However, many of the base beams were immobilized in a parallel configuration, indicating that a canvas had been present when the structure bound the surface (fig. S4). Transient assembly of canvas and frame may be useful for positioning devices such that the sleeve has free access to the surface.

Programmable positioning in 2D

To control the position of the sleeve in 2D, each of the two base beams and the sliding rail of the frame is decorated with a track comprising nine unique single-stranded address strands as origami staple extensions. Address strands are also incorporated at the ends of the rail beams and at the ends of the sleeve (Fig. 2A and fig. S5). By adding two bridging strands that link sleeve and rail addresses, we can bind the sleeve to a programmed position between two address sites (straddling an intermediate site); using separate pairs of bridging strands, we can similarly position the rail between any pair of adjacent address sites along the base beams. Sleeve and rail can thus each be locked in seven and eight positions, respectively, giving

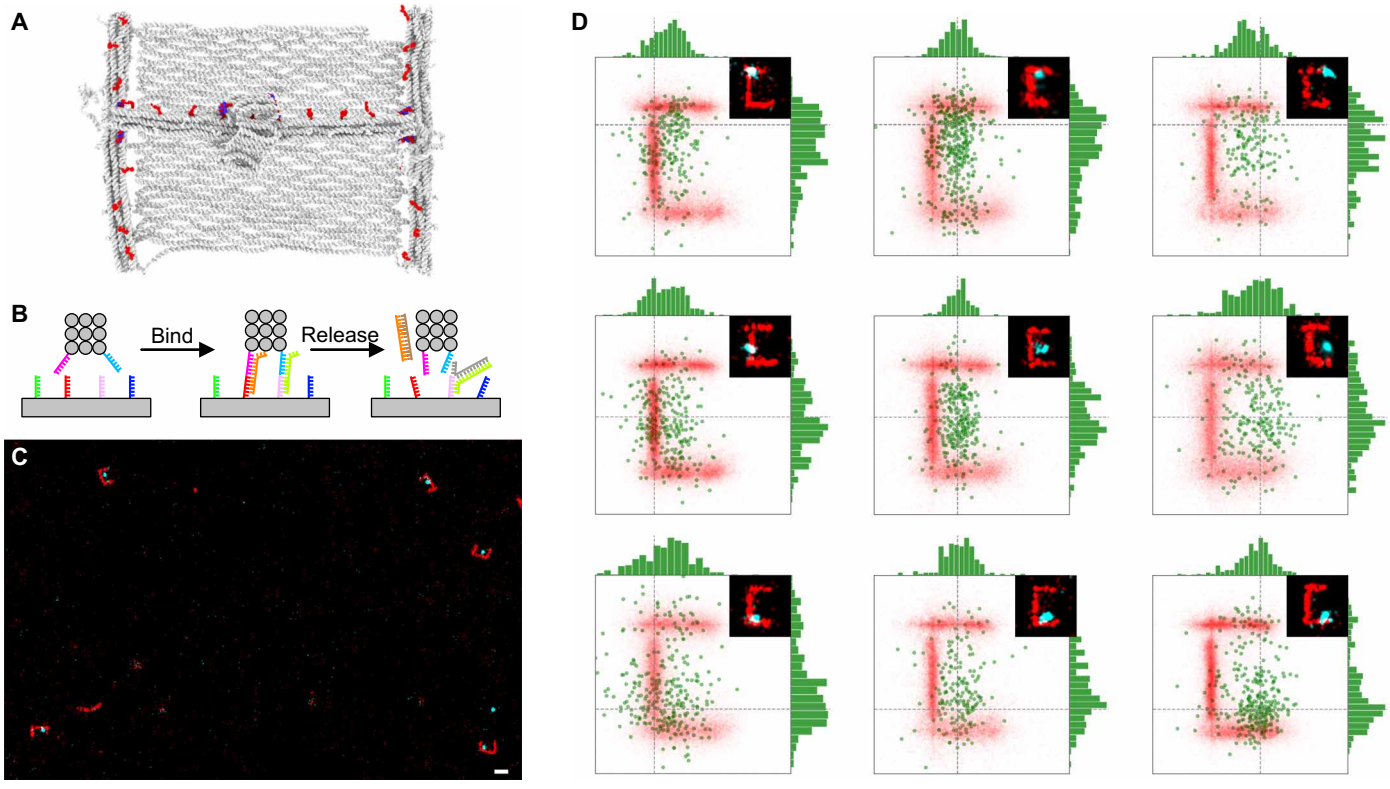

Fig. 2. Controlled 2D positioning. (**A**) The device is decorated with tracks of unique, single-stranded address strands (red). (**B**) By selectively linking pairs of address strands on the base beams, rail, and sleeve the write head can be positioned in 2D. Links are reversible through toehold-mediated strand displacement. (**C**) DNA-PAINT image of devices with the sleeve positioned in the center (frame and canvas are red, sleeve is blue). Scale bar, 100 nm. (**D**) Sleeve positions from aligned DNA-PAINT images of devices with write head positioned in nine different locations: Each green point corresponds to the mean position of the sleeve of one device. Insets show examples of DNA-PAINT images. Plot windows are 200 nm by 200 nm.

a grid of 56 positions, separated by ~10 nm, of the sleeve over the canvas.

To be able to add and remove binding strands, we performed positioning experiments using structures immobilized in glass-bottom flow chambers. We removed one line of DNA-PAINT docking sites on the canvas and the line on the rail arm to create a "C"-shaped pattern that allows us to determine the position of the sleeve in relation to the frame and canvas. A complicating factor is that the sleeve can unthread the rail and move onto either of the single-stranded scaffold linkers connecting the rail to the base beams: If the beam is then locked to the base, the sleeve will not be able to move back onto the rail. The sleeve must therefore be locked onto the rail before the rail is locked to the base. In early positioning experiments, most sleeves were trapped in a linker region at the top or bottom of the frame. We suspected that electrostatic repulsion between sleeve and rail played a role in preventing the sleeve from threading onto the rail, so we increased the concentration of divalent cations in the buffer used for positioning (fig. S6). At 25 mM $MgCl_2$, we could see the sleeve successfully threading the rail. Figure 2 shows the results of tests in which we used three positions each for sleeve and rail—that is, nine possible write-head positions. Using DNA-PAINT, we are able to capture wide-field images containing hundreds of devices. We selected devices where a sleeve is present (85% yield) and used a script to fit fluorescence localizations corresponding to docking sites on the frame and canvas to rotate and align data from multiple structures to create averaged images (fig. S7). Fifty-one percent of sleeves were localized in their programmed positions (figs. S8 to S17). We also tested positioning based on the polar coordinate system of the bow and arrow device (fig. S18).

To be able to reposition the write head, all bridging strands incorporate a 6-nt overhang to enable their removal by toehold-mediated strand displacement (*28*) on addition of a completely complementary removal strand. Because we have independent control of the two axes of motion, we can choose to release just one axis (sleeve or rail) or both at the same time. We attempted to release and reposition the sleeve while keeping the rail locked, thus ensuring that the sleeve remained threaded on the rail. This strategy had low yield: Many sleeves remained in their original positions, probably due to nonspecific interactions between canvas and sleeve when the rail is locked down (fig. S19). By moving the sleeve after releasing the rail, giving it enough clearance to move freely, we were able to reposition the sleeve in 2D (Fig. 3A). We then positioned the same device four times sequentially to move between the four corners of the canvas (Fig. 3B) and were able to see the corresponding movement of the sleeve.

Programmed patterning through DNA strand–displacement reactions

Our goal was to use the 2D positioning system as a prototype printer by adding write-head functionality to the sleeve. We implemented an all-DNA surface patterning system. We functionalized the sleeve with a protruding strand that acts as a catalyst for toehold-mediated strand exchange (*28*). The top of the canvas was decorated with 56 pixels spaced 10 nm apart comprising identical extensions of

56 staples (fig. S20). Each pixel strand was initially hybridized to a blocking strand, leaving a 6-nt single-stranded toehold exposed (Fig. 4A). The write-head catalyst is capable of binding to this toehold and partially displacing the blocking strand to reveal a second toehold on the pixel strand, which is initially hidden in a bulge in the pixel strand–blocker duplex. The ink strand is fully complementary to the revealed toehold and to the flanking domains of the pixel strand covered by the blocker: Hybridization of the ink strand to the revealed toehold initiates its displacement of both blocker and catalyst (*28*). The initial site-specific interaction of the catalyst with the pixel-blocker duplex, which is transient and reversible, thus catalyzes complete removal of the blocker by an ink strand. By using the write head to catalyze addition of functionalized ink strands at selected sites, the canvas could be decorated by, for example, fluorophores, nanoparticles, or proteins. Here, to enable the written pattern to be imaged, the ink strand contained a DNA-PAINT docking domain.

The pixel-modifying strand-displacement reaction was characterized by adding fluorophore-labeled ink strands, with or without free strand-exchange catalysts, to pixel-decorated canvases in solution. Canvases were then separated from ink by gel electrophoresis, and the incorporation of the ink strand in the canvas was monitored by measuring fluorescence from the corresponding gel band. We observed a low background incorporation of ink when no catalyst was present and up to 60 times increase in incorporation with increasing catalyst concentration (fig. S21). When complete devices incorporating the pixelated canvas were immobilized in a flow chamber, the rate of leak reaction leading to background patterning on our canvases was higher than expected from the solution-based controls (fig. S22). It was nevertheless possible to distinguish patterns with two sites on the canvas selectively modified by sequential positioning of the write head (Fig. 4C).

DISCUSSION

Positioning precision is difficult to estimate from PAINT images, in which imprecision in device operation is convolved with uncertainty in PAINT localization. The Exchange-PAINT (*27*) measurements presented here rely on localization of the frame in one imaging step to provide a reference coordinate system to assess write-head and ink positioning recorded in later steps. Microscope drift during exchange of the imaging strand and buffer, and during imaging, is corrected using gold nanoparticles as fiducial markers, but errors in the alignment of sequentially recorded images of frame, write head, and ink are greater than imaging uncertainty achievable using a single PAINT channel. Rotation and alignment of data from multiple devices, and structural variations resulting from the flexibility of the canvas and of its linkages to the two base beams, introduce further distortion. A better way to assess device operation would be to use the 10-nm pattern of modified pixels to provide its own coordinate system to measure positioning errors; this will require optimization of the writing operation to enable modification of multiple pixels.

We used coarse-grained molecular dynamics simulations (*29*, *30*) to simulate the device when locked into position (fig. S23) and found that play in the device is anisotropic, around 5 nm along the rail axis and 2.5 nm orthogonal to it. The play of the rail arm is mostly along its axis, attributable to the linkage to the base frame. Motion of the sleeve relative to the rail is more isotropic and is associated with the relatively large clearance between sleeve and rail.

We can draw several mechanical design lessons. While the assembled sleeve remained topologically locked to the frame, its control was complicated by the omission of bulky stoppers to keep it from sliding off the rail onto flexible linker domains. Future designs could incorporate stoppers made from DNA tiles (*31*) to retain the sleeve while conserving scaffold material. Stoppers may increase the speed of repositioning by limiting motion of the slider. We made our device as large as possible, given the number of origami components, to enable reliable characterization by optical microscopy: A smaller device incorporating more rigid DNA origami beams might achieve higher precision on a smaller canvas. Precision could also be enhanced by reducing the flexibility of linkages between components and by experimental optimization of sleeve and rail to minimize play while ensuring that the sleeve loads effectively and moves freely. The pixel writing operation could be more tightly localized by moving the toehold engaged by the strand-exchange catalyst to the other end of the pixel duplex, next to the origami substrate.

The printer is a Brownian ratchet (*32*) that relies on diffusion to explore possible binding positions and hybridization of signaling oligonucleotides to alternately release components and lock them

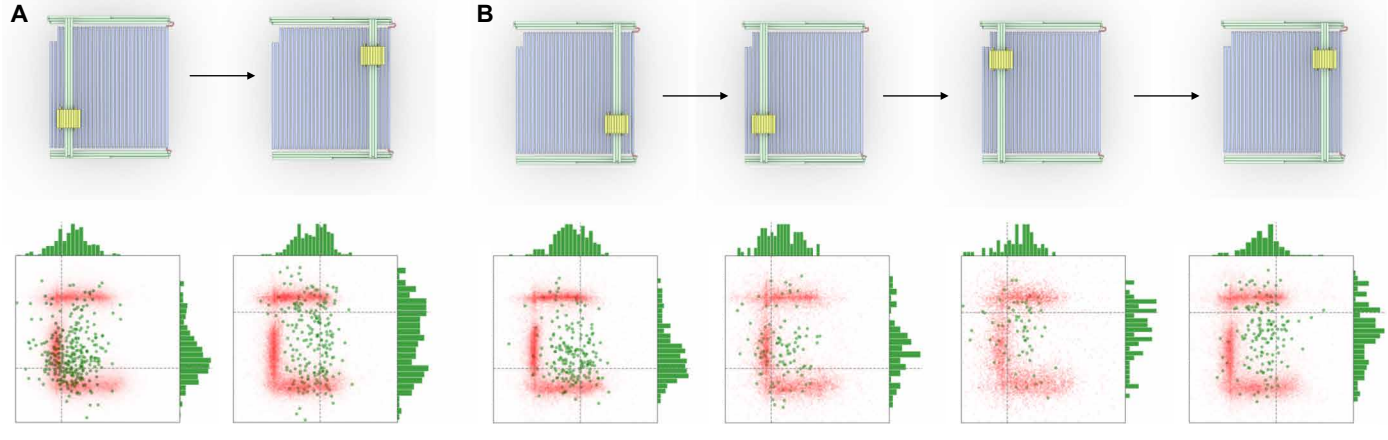

Fig. 3. Programmed 2D motion of sleeve. Top, schematic illustrations of sleeve position; bottom, corresponding positions measured from aligned DNA-PAINT images of devices. Each green point corresponds to the mean position of the sleeve of one device. Plot windows are 200 nm by 200 nm. (**A**) Diagonal motion through release and rebinding of both sleeve and rail. (**B**) Four consecutive steps of the sleeve.

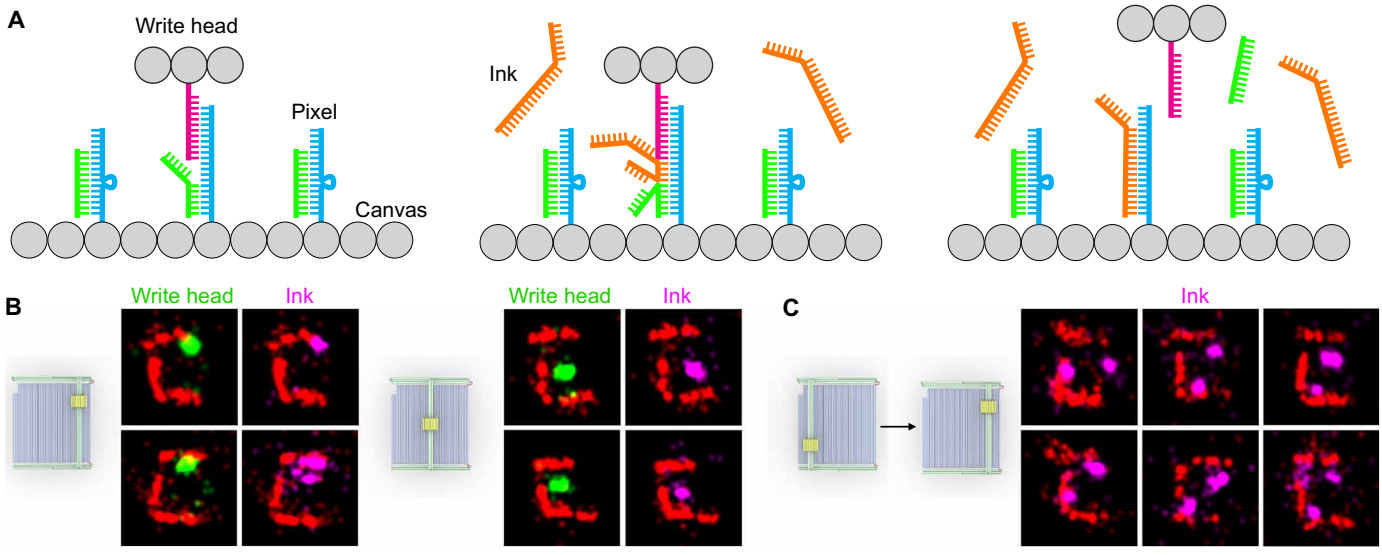

Fig. 4. Programmed printing. (**A**) Schematic diagrams show printing by means of a toehold catalyst, carried by the write head, which enables local incorporation of an ink strand (orange) through a strand-displacement reaction. (**B**) Examples of printing a single dot, in the top right corner and center of the canvas: slider localization in green and ink localization in magenta. (**C**) Examples of sequential printing of two dots in diagonally opposite corners of the canvas on the same device. The ink is imaged after the second printing step. All data cropped in 200-nm boxes.

in place. There is considerable scope for optimization of the cycle time. The limiting step is likely to be the toehold-mediated strand displacement used for release. The rate constant for these reactions could be increased to ~10^6 M^{-1} s^{-1} by increasing toehold lengths (*33*), potentially decreasing repositioning times to a few seconds for typical micromolar strand concentrations if interfaced to a microfluidic signal delivery system. Nanostructures actuated by light (*17*), electric (*12*), or magnetic (*18*) fields can respond more rapidly to external signals, but it would be difficult to achieve the same fine control of positioning that can be achieved by use of information-bearing signaling molecules to encode positioning instructions.

Characterization of the printing on the canvas by means of the write head was limited by a background of off-target ink incorporation. This could be improved by optimization or redesign of the strand-displacement reaction (*34*, *35*) to reduce leakage; by use of the write head to produce a localized covalent reaction between co-localized reactants (*36*–*38*); or by positioning a catalyst, sensitizer (*39*), or enzyme (*40*, *41*). Direct modification of the surface to which the device is bound could be achieved using a porous wireframe canvas (*42*) or by removing the canvas after deposition.

Externally controlled motion at the nanoscale is an important goal for molecular nanotechnology. In this work, we have drawn inspiration from macroscale engineering by coupling multiple linear positioning elements to create a DNA nanomanipulator capable of programmable 2D motion. Our devices exemplify characteristic strengths of DNA nanotechnology—programmable assembly and orthogonal control of structural transitions through sequence-specific strand-displacement reactions to steer motion. We show that multiple DNA origami positioning elements can be combined and independently controlled. We also show that the positioner is capable of acting as a molecular printer by using the write head to catalyze local incorporation of a fluorescent label. Although these first-generation devices are slow and limited in function, their low cost, extreme scalability through parallelization, and compatibility with aqueous conditions make such devices attractive for development toward applications in nanoscale additive manufacturing.

MATERIALS AND METHODS

DNA nanostructure design

Individual nanostructure components were designed using caDNAno (*43*) on a square lattice with deletions every 42 bp for twist correction. The canvas and frame were designed around the 8064-nt p8064 scaffold; the sleeve was designed around a 1496-nt restriction digest fragment from the same scaffold. The canvas was designed around 30 parallel helices threaded by the scaffold. In the frame, the scaffold is divided between top and bottom base beams, rail beam, and three linker regions joining them. The linker joining the two base beams runs parallel to a helix at the edge of the canvas and is joined to it by 10 staple extensions that cross over between scaffolds to form 3-bp duplexes. The two linkers between the rail beam and base beams are each 237 nt in length. To maximize the flexibility in these regions, we used mfold (*44*) to calculate secondary structure free energies for all pairs of 237-nt scaffold domains separated by 2767 nt (the length of scaffold in the rail) and selected the pair for which the secondary structure free energy of the highest member of the pair is minimal. To further reduce the risk of strong secondary structure in the linkers, we added 16-nt staples every 32 nt to make them partially double stranded. The sleeve was designed as a flat 22-helix sheet with three four-helix double-layer regions.

After initial design in caDNAno, all structures were imported to a single vHelix (*45*) file to design the interstructure linkages. Helices of the base beams and canvas are orthogonal. The canvas is connected to each base rail through staple links from the rail to the ends of four canvas helices. Links were initially designed by assuming a helix-to-helix spacing in the canvas of 3 nm (*46*); designs were simulated in oxDNA, and the linkages were manually reconfigured to minimize strain between frame and canvas. All scaffold and staple

sequences—as well as the sequences of protruding staple extensions used for sleeve loading, positioning, and DNA-PAINT docking sites—were assigned in vHelix.

DNA nanostructure assembly

Scaffold strands (p8064) were purchased from tilibit nanosystems GmbH. Staple strands were purchased from Integrated DNA Technologies Inc. The linear 1496-nt scaffold fragment was prepared by mixing 50 μl of scaffold (100 nM) with a 20× excess of 20- and 30-nt oligonucleotides, complementary to the scaffold in the regions to be digested, in NEB CutSmart buffer; 90-min incubation with 5 μl (20 U μl^{-1}) of XmnI restriction enzyme (NEB) at 37°C; 90-min incubation at 60°C with 5 μl (10 U μl^{-1}) of BsaBI (NEB); and 20-min incubation at 80°C to heat-inactivate the enzymes. All structures were folded with a scaffold concentration of 5 nM and a staple concentration of 50 nM (each) in Tris-EDTA (TE) buffer with 10 mM $MgCl_2$. The folding protocol started with a 5-min incubation at 80°C followed by a rapid decrease to 60°C over 20 min and slow cooling to 20°C over 14 hours.

After folding, structures were purified from excess staple strands using PEG precipitation (*25*). Separately, 300 μl of canvas and frame sample and 450 μl of sleeve sample were each diluted to 500 μl in 1.5-ml centrifuge tubes using folding buffer; 5 μl of 1 M $MgCl_2$ was added to bring the $MgCl_2$ concentration up to 20 mM. After this, 500 μl of PEG precipitation mixture was added [1× TE, 10 mM $MgCl_2$, 15% (w/v) PEG-8000, and 500 mM NaCl]. Samples were centrifuged at 20,000*g* for 25 min, and the supernatant was immediately removed. The pellet was resuspended in folding buffer (supplemented to 20 mM $MgCl_2$), and the process was repeated. After removing the supernatant, the frame was resuspended in 225 μl of folding buffer with 10 mM $MgCl_2$, the sleeve was resuspended in 300 μl of folding buffer with 10 mM $MgCl_2$, and the canvas was resuspended in 225 μl of folding buffer, with the magnesium concentration reduced to 5 mM $MgCl_2$. After adding the buffers, the samples were placed in a 37°C water bath for 1 hour to resuspend the pellet. When a canvas with print pixels was used, a blocker strand (50× excess with respect to pixel strands) was then added to block the pixels for printing and the sample was incubated for a further 1 hour in the water bath.

Devices were assembled by mixing the frame, canvas, and sleeve, each at a concentration of about 5 nM in a 1:1:1.38 ratio; adding $MgCl_2$ to bring the concentration up to 12 mM; and incubating at 37°C for 72 hours to link the structures. The sleeve was then closed around the rail by adding a 4× excess of seam strands (3.96 μl at 1 μM each added to 660 μl of device mixture) and incubating at 37°C for 24 hours. The sleeve was then released from the rail by addition of 2.25 μl of invader strands (33.3 μM each) to 640 μl of device mixture and incubation at 37°C for 3 hours. To enrich devices with a sleeve, 150 μl of poly-T magnetic beads [Dynabeads Oligo(dT)25, Thermo Fisher Scientific] at the supplied concentration was placed on a magnetic rack and the supernatant was removed. The device sample was added to the beads, and the mixture was put on a rotary mixer overnight at room temperature to capture device structures on the beads. The beads were then washed four times with 400 μl of folding buffer and resuspended in 150 μl of folding buffer. To release the structures from the beads, 4 μl of 100 μM release invaders was added and the samples were incubated for 3 hours at room temperature on a rotary mixer. The final sample was split into 10-μl aliquots for further experiments.

Transmission electron microscopy

Samples were diluted to about 1 nM and deposited on glow-discharged formvar-supported carbon-coated Cu300 TEM grids (Agar Scientific). A pseudo-positive staining method was used, whereby the grids were incubated with the sample for 2 min, blotted with filter paper, and then incubated for 3 s on a drop of water. This was followed by a 20-s incubation on a 20-μl drop of 2% uranyl acetate. After blotting, the sample was placed for 3 s on another drop of water followed by filter blotting and air drying. Samples were imaged in a FEI Tecnai T12 microscope (120 kV), and images were recorded on a 16-megapixel Gatan OneView camera.

Device positioning

A 10-μl aliquot of bead-purified structures was diluted with 40 μl of buffer B+ (*26*) (10 mM $MgCl_2$, 5 mM tris, 1 mM EDTA, and 0.05% Tween 20). An ibidi sticky-Slide VI 0.4 (ibidi GmbH) was attached to an oven-baked #1.5 glass coverslip to form flow channels. The flow channels include reservoirs at the top and bottom that were used as inlet and outlet: Buffer replacement was performed by adding new solutions to one reservoir and removing buffer from the other by direct pipetting; when the reservoirs were emptied, the flow channel itself remained filled with buffer. To one channel, 80 μl of biotinylated bovine serum albumin (BSA) solution {biotinylated BSA (1 mg ml^{-1}; Merck Life Science) in buffer A+ [10 mM tris-HCl, 100 mM NaCl, and 0.05% (v/v) Tween 20 at pH 8.0]} was added and incubated for 5 min. The channel was then emptied and washed with 180 μl of buffer A+ followed by addition of 40 μl of streptavidin solution [streptavidin (0.5 mg ml^{-1}; Thermo Fisher Scientific) in buffer A+]. The streptavidin solution was incubated for 5 min and then removed and replaced, followed by a further 5-min incubation. The channel was again washed with 180 μl of buffer A+. A 50-μl sample of gold nanoparticles (60 nm; BBI Solutions) was diluted in 50 μl of buffer A+, and 50 μl of this was immediately added to the channel and incubated for 2 min. The channel was then washed with 180 μl of buffer A+ and 180 μl of buffer B+, followed by the addition of the diluted DNA sample. The chamber slide was capped with the included lid, incubated on an orbital shaker at room temperature for 60 min, and then washed with 180 μl of B+ buffer to remove nonbound devices.

To position the sleeve on the rail, a linker mixture was prepared with 0.5 nM each of the address linkers in buffer B+ with 25 mM $MgCl_2$. To make sure that the devices were equilibrated in this solution, 100 μl was first added to the inlet reservoir and removed from the outlet reservoir followed by the addition of a further 100 μl. The flow channels were then plugged and the slide was placed in a 37°C incubator overnight, followed by double washing with 180 μl of buffer B+. To position the rail on the frame base, address strand mixtures were prepared with 5 nM each of the linkers in buffer B+ with 25 mM $MgCl_2$. Again, 100 μl of this mixture was added and removed, followed by the addition of a further 100 μl to equilibrate the devices in the buffer. The slide was closed and incubated at 37°C for 1 hour.

The sleeve and rail can be released separately or at the same time. A mixture of 5 μM each of the release strands was prepared in buffer B+. The channel was equilibrated to the invader mixture by adding and removing 100 μl, followed by the addition of 100 μl. The slide was closed using the included lid and incubated at 37°C for 1 hour.

The canvas was patterned by diluting an ink strand functionalized with a R3 DNA-PAINT docking site in buffer B+ with 30 mM $MgCl_2$.

This mixture was added to the channel by first adding and removing 100 µl and then adding a further 100 µl. All patterning experiments were performed by incubating the mixture in the channel for 10 min at room temperature followed by washing three times with 180 µl of buffer B+. The quantity of ink needed was titrated by locking the device in place and adding successively higher concentrations of ink—first 1 nM and then 5 and 10 nM. DNA-PAINT was used to image frame, sleeve, and ink after each addition. For patterning in multiple positions, a solution with 10 nM ink was added for 10 min after the sleeve had been positioned.

DNA-PAINT microscopy

DNA-PAINT imager strands functionalized with Cy3B were purchased from Eurofins Genomics. Imaging buffer was prepared by adding Trolox (0.25 mg ml^{-1}; MP Biomedicals), protocatechuic acid (0.385 mg ml^{-1}; MP Biomedicals), and protocatechuate 3,4-dioxygenase (7 µg ml^{-1}; MP Biomedicals) to buffer B+. An Oxford Nanoimager S microscope was used in total internal reflection fluorescence mode to image the samples with a 532-nm laser. One hundred microliters of imager strands was added to the slide channel: Imaging strand P1 (CTAGATGTAT-CY3B) was used at 4 nM to image the frame and canvas; R1(AGGAGGA-CY3B) was used at 1 nM to image the sleeve; and R3 (GAGAGAG-CY3B) was used at 2 nM to image patterning. A 200-ms exposure time was used, with 12,000/5000/8000 frames recorded for the frame/sleeve/patterning. Between imaging rounds, the channel was washed twice with 180 µl of buffer B+. The data were reconstructed using Picasso (*26*) with the "lq" fit method and a gradient of 5000. Drift correction was performed using the redundant cross correlation method with a segment size of 200 frames. Localizations were linked with a maximum distance of one pixel and a maximum of one transient dark frame.

SUPPLEMENTARY MATERIALS

www.science.org/doi/10.1126/scirobotics.abn5459
Figs. S1 to S23
Tables S1 to S6
Data files S1 and S2

REFERENCES AND NOTES

1. K. E. Drexler, Molecular engineering: An approach to the development of general capabilities for molecular manipulation. *Proc. Natl. Acad. Sci. U.S.A.* **78**, 5275–5278 (1981).
2. K. E. Drexler, *Nanosystems: Molecular Machinery, Manufacturing, and Computation* (Wiley, 1992).
3. J. A. Stroscio, D. M. Eigler, Atomic manipulation. *Science* **254**, 1319–1326 (1991).
4. R. Achal, M. Rashidi, J. Croshaw, D. Churchill, M. Taucer, T. Huff, M. Cloutier, J. Pitters, R. A. Wolkow, Lithography for robust and editable atomic-scale silicon devices and memories. *Nat. Commun.* **9**, 2778 (2018).
5. P. Vettinger, M. Despont, U. Drechsler, U. Dürig, W. Häberle, M. I. Lutwyche, H. E. Rothuizen, R. Stutz, R. Widmer, G. K. Binnig, The "Millipede"—More than thousand tips for future AFM storage. *IBM J. Res. Dev.* **44**, 323–340 (2000).
6. N. C. Seeman, Nucleic acid junctions and lattices. *J. Theor. Biol.* **99**, 237–247 (1982).
7. P. W. K. Rothemund, Folding DNA to create nanoscale shapes and patterns. *Nature* **440**, 297–302 (2006).
8. A. E. Marras, L. Zhou, H.-J. Su, C. E. Castro, Programmable motion of DNA origami mechanisms. *Proc. Natl. Acad. Sci. U.S.A.* **112**, 713–718 (2015).
9. J. List, E. Falgenhauer, E. Kopperger, G. Pardatscher, F. C. Simmel, Long-range movement of large mechanically interlocked DNA nanostructures. *Nat. Commun.* **7**, 12414 (2016).
10. J. T. Powell, B. O. Akhuetie-oni, Z. Zhang, C. Lin, DNA origami rotaxanes: Tailored synthesis and controlled structure switching. *Angew. Chem. Int. Ed.* **55**, 11412–11416 (2016).
11. E. Benson, R. Carrascosa Marzo, J. Bath, A. J. Turberfield, Strategies for constructing and operating DNA origami linear actuators. *Small* **17**, 2007704 (2021).
12. E. Kopperger, J. List, S. Madhira, F. Rothfischer, D. C. Lamb, F. C. Simmel, A self-assembled nanoscale robotic arm controlled by electric fields. *Science* **359**, 296–301 (2018).
13. P. Ketterer, E. M. Willner, H. Dietz, Nanoscale rotary apparatus formed from tight-fitting 3D DNA components. *Sci. Adv.* **2**, e1501209 (2016).
14. J. J. Funke, H. Dietz, Placing molecules with Bohr radius resolution using DNA origami. *Nat. Nanotechnol.* **11**, 47–52 (2016).
15. E. S. Andersen, M. Dong, M. M. Nielsen, K. Jahn, R. Subramani, W. Mamdouh, M. M. Golas, B. Sander, H. Stark, C. L. P. Oliveira, J. S. Pedersen, V. Birkedal, F. Besenbacher, K. V. Gothelf, J. Kjems, Self-assembly of a nanoscale DNA box with a controllable lid. *Nature* **459**, 73–76 (2009).
16. R. P. Goodman, M. Heilemann, S. Doose, C. M. Erben, A. N. Kapanidis, A. J. Turberfield, Reconfigurable, braced, three-dimensional DNA nanostructures. *Nat. Nanotechnol.* **3**, 93–96 (2008).
17. Y. Yang, M. Endo, K. Hidaka, H. Sugiyama, Photo-controllable DNA origami nanostructures assembling into predesigned multiorientational patterns. *J. Am. Chem. Soc.* **134**, 20645–20653 (2012).
18. S. Lauback, K. R. Mattioli, A. E. Marras, M. Armstrong, T. P. Rudibaugh, R. Sooryakumar, C. E. Castro, Real-time magnetic actuation of DNA nanodevices via modular integration with stiff micro-levers. *Nat. Commun.* **9**, 1446 (2018).
19. T. Gerling, K. F. Wagenbauer, A. M. Neuner, H. Dietz, Dynamic DNA devices and assemblies formed by shape-complementary, non-base pairing 3D components. *Science* **347**, 1446–1452 (2015).
20. H. Ijäs, I. Hakaste, B. Shen, M. A. Kostiainen, V. Linko, Reconfigurable DNA origami nanocapsule for pH-controlled encapsulation and display of cargo. *ACS Nano* **13**, 5959–5967 (2019).
21. S. M. Douglas, I. Bachelet, G. M. Church, A logic-gated nanorobot for targeted transport of molecular payloads. *Science* **335**, 831–834 (2012).
22. A. Kuzuya, Y. Sakai, T. Yamazaki, Y. Xu, M. Komiyama, Nanomechanical DNA origami "single-molecule beacons" directly imaged by atomic force microscopy. *Nat. Commun.* **2**, 449 (2011).
23. S. M. Douglas, H. Dietz, T. Liedl, B. Högberg, F. Graf, W. M. Shih, Self-assembly of DNA into nanoscale three-dimensional shapes. *Nature* **459**, 414–418 (2009).
24. K. F. Wagenbauer, C. Sigl, H. Dietz, Gigadalton-scale shape-programmable DNA assemblies. *Nature* **552**, 78–83 (2017).
25. E. Stahl, T. G. Martin, F. Praetorius, H. Dietz, Facile and scalable preparation of pure and dense DNA origami solutions. *Angew. Chem. Int. Ed.* **53**, 12735–12740 (2014).
26. J. Schnitzbauer, M. T. Strauss, T. Schlichthaerle, F. Schueder, R. Jungmann, Super-resolution microscopy with DNA-PAINT. *Nat. Protoc.* **12**, 1198–1228 (2017).
27. R. Jungmann, M. S. Avendaño, J. B. Woehrstein, M. Dai, W. M. Shih, P. Yin, Multiplexed 3D cellular super-resolution imaging with DNA-PAINT and Exchange-PAINT. *Nat. Methods* **11**, 313–318 (2014).
28. B. Yurke, A. J. Turberfield, A. P. Mills, F. C. Simmel, J. L. Neumann, A DNA-fuelled molecular machine made of DNA. *Nature* **406**, 605–608 (2000).
29. T. E. Ouldridge, A. A. Louis, J. P. K. Doye, Structural, mechanical, and thermodynamic properties of a coarse-grained DNA model. *J. Chem. Phys.* **134**, 085101 (2011).
30. E. Poppleton, J. Bohlin, M. Matthies, S. Sharma, F. Zhang, P. Sulc, Design, optimization and analysis of large DNA and RNA nanostructures through interactive visualization, editing and molecular simulation. *Nucleic Acids Res.* **48**, e72 (2020).
31. Y. Ke, L. L. Ong, W. M. Shih, P. Yin, Three-dimensional structures self-assembled from DNA bricks. *Science* **338**, 1177–1183 (2012).
32. H. Wang, G. Oster, Ratchets, power strokes, and molecular motors. *Appl. Phys. A Mater. Sci. Process.* **75**, 315–323 (2002).
33. D. Y. Zhang, E. Winfree, Control of DNA strand displacement kinetics using toehold exchange. *J. Am. Chem. Soc.* **131**, 17303–17314 (2009).
34. L. Qian, E. Winfree, Scaling up digital circuit computation with DNA strand displacement cascades. *Science* **332**, 1196–1201 (2011).
35. B. Wang, C. Thachuk, A. D. Ellington, E. Winfree, D. Soloveichik, Effective design principles for leakless strand displacement systems. *Proc. Natl. Acad. Sci. U.S.A.* **115**, E12182–E12191 (2018).
36. Z. J. Gartner, D. R. Liu, The generality of DNA-templated synthesis as a basis for evolving non-natural small molecules. *J. Am. Chem. Soc.* **123**, 6961–6963 (2001).
37. Y. He, D. R. Liu, Autonomous multistep organic synthesis in a single isothermal solution mediated by a DNA walker. *Nat. Nanotechnol.* **5**, 778–782 (2010).
38. W. Meng, R. A. Muscat, M. L. McKee, P. J. Milnes, A. H. El-Sagheer, J. Bath, B. G. Davis, T. Brown, R. K. O'Reilly, A. J. Turberfield, An autonomous molecular assembler for programmable chemical synthesis. *Nat. Chem.* **8**, 542–548 (2016).
39. S. Helmig, A. Rotaru, D. Arian, L. Kovbasyuk, J. Arnbjerg, P. R. Ogilby, J. Kjems, A. Mokhir, F. Besenbacher, K. V. Gothelf, Single molecule atomic force microscopy studies of photosensitized singlet oxygen behavior on a DNA origami template. *ACS Nano* **4**, 7475–7480 (2010).
40. O. I. Wilner, Y. Weizmann, R. Gill, O. Lioubashevski, R. Freeman, I. Willner, Enzyme cascades activated on topologically programmed DNA scaffolds. *Nat. Nanotechnol.* **4**, 249–254 (2009).

41. J. Fu, M. Liu, Y. Liu, N. W. Woodbury, H. Yan, Interenzyme substrate diffusion for an enzyme cascade organized on spatially addressable DNA nanostructures. *J. Am. Chem. Soc.* **134**, 5516–5519 (2012).
42. E. Benson, A. Mohammed, A. Bosco, A. I. Teixeira, P. Orponen, B. Högberg, Computer-aided production of scaffolded DNA nanostructures from flat sheet meshes. *Angew. Chem. Int. Ed.* **55**, 8869–8872 (2016).
43. S. M. Douglas, A. H. Marblestone, S. Teerapittayanon, A. Vazquez, G. M. Church, W. M. Shih, Rapid prototyping of 3D DNA-origami shapes with caDNAno. *Nucleic Acids Res.* **37**, 5001–5006 (2009).
44. M. Zuker, Mfold web server for nucleic acid folding and hybridization prediction. *Nucleic Acids Res.* **31**, 3406–3415 (2003).
45. E. Benson, A. Mohammed, J. Gardell, S. Masich, E. Czeizler, P. Orponen, B. Högberg, DNA rendering of polyhedral meshes at the nanoscale. *Nature* **523**, 441–444 (2015).
46. X.-C. Bai, T. G. Martin, S. H. W. Scheres, H. Dietz, Cryo-EM structure of a 3D DNA-origami object. *Proc. Natl. Acad. Sci. U.S.A.* **109**, 20012–20017 (2012).

Acknowledgments: We thank W. Shih (Wyss Institute, Harvard University) and L. Kilwing (Faculty of Physics, Ludwig Maximilian University, Munich) for helpful discussions and E. Drexler (Future of Humanity Institute, University of Oxford) for inspiration. **Funding:** This material is based on the work supported by the U.S. Department of Energy's Office of Energy Efficiency and Renewable Energy (EERE) under the Advanced Manufacturing Office Award Number DE-EE0008310. E.B. is supported by a Marie Skłodowska-Curie Individual Fellowship (grant agreement no. 842291). R.C.M. is supported by the European Union's Horizon 2020 research and innovation programme through the Marie Skłodowska-Curie "DNA-Robotics" Innovative Training Network (grant agreement no. 765703). Disclaimer: This report was prepared as an account of work sponsored by an agency of the U.S. government. Neither the U.S. government nor any agency thereof, nor any of their employees, makes any warranty, express or implied; assumes any legal liability or responsibility for the accuracy, completeness, or usefulness of any information, apparatus, product, or process disclosed; or represents that its use would not infringe privately owned rights. Reference herein to any specific commercial product, process, or service by trade name, trademark, manufacturer, or otherwise does not necessarily constitute or imply its endorsement, recommendation, or favoring by the U.S. government or any agency thereof. The views and opinions of authors expressed here do not necessarily state or reflect those of the U.S. government or any agency thereof. **Author contributions:** The project was conceived by A.J.T. Implementation was designed by all authors. Experiments were performed by E.B. and R.C.M. Simulations and data analysis were performed by E.B. The manuscript was drafted by E.B. and A.J.T. and reviewed and edited by J.B. and R.C.M. **Competing interests:** The authors declare that they have no competing interests. **Data and materials availability:** All data needed to evaluate the conclusions in the paper are present in the paper or the Supplementary Materials. Microscope data are available at https://doi.org/10.5287/bodleian:VY6OebymR.

Submitted 3 December 2021
Accepted 28 March 2022
Published 20 April 2022
10.1126/scirobotics.abn5459

Science Robotics

A DNA molecular printer capable of programmable positioning and patterning in two dimensions

Erik Benson, Rafael Carrascosa Marzo, Jonathan Bath, and Andrew J. Turberfield

Sci. Robot. **7** (65), eabn5459. DOI: 10.1126/scirobotics.abn5459

Science Robotics (ISSN 2470-9476) is published by the American Association for the Advancement of Science. 1200 New York Avenue NW, Washington, DC 20005. The title *Science Robotics* is a registered trademark of AAAS.